

**Supporting Information**  
**for**  
**An Inverse NiO<sub>1-x</sub>/Cu Catalyst with High Activity towards**  
**Water-Gas Shift**

Li-Yong Gan<sup>1,2</sup>, Wei-Xue Li<sup>3</sup>, Yu-Jun Zhao<sup>1,2,\*</sup>

**Computational Details**

This work was conducted by the Vienna Ab Initio Simulation Package (VASP)<sup>1</sup> with the frozen-core projector-augmented-wave (PAW) method<sup>2</sup>. The spin-polarized Perdew Wang (PW91) generalized gradient approximation (GGA)<sup>3</sup> functional was employed for the exchange-correlation energy. A cutoff energy of 500eV was employed for the plane-wave expansion. The three surfaces, clean Cu(111), CuNi(111), and inverse NiO<sub>1-x</sub>/Cu(111) were modeled with a  $p(2\sqrt{3}\times 2\sqrt{3})R30^\circ$  supercell, which is large enough to avoid the lateral interaction. A 4-layer slab with a vacuum of 15 Å was used, and a 5×5×1  $\Gamma$ -centered  $k$ -point mesh was sampled for the reciprocal space. Convergence test with regard to the  $k$ -points, energy cutoff and vacuum thickness have been carefully performed<sup>4</sup>. The CuNi(111) bimetallic surface was modeled with non-contiguous Ni pairs homogeneously distributed on the surface layer and each Ni atom surrounded by six Cu atoms on the basis of our previous results<sup>5</sup> [c.f. Fig. S1 (c)], while the NiO<sub>1-x</sub>/Cu(111) was modeled with a chain of nanoparticles deposited on Cu(111) similar to what Liu proposed for oxide/Cu systems in Ref. 6 [c.f. Fig. S1 (a) and (b)]. The adsorbed molecules were put on one side of the slab. The positions of all atoms except those in the two bottommost layers were fully relaxed with the residual forces less than 0.02eV/Å. The lattice constant of Cu were optimized to 3.64 Å.

Energy barriers and minimum energy paths (MEPs) have been computed using the climbing-image nudged elastic band (CI-NEB)<sup>7</sup>. The reaction barriers of the elementary reaction steps were calculated with respect to the most stable adsorbed states of the reactants. After the transition state (TS) searching, the TS was further optimized by the quasi-Newton method until the residual forces were less than 0.02 eV/Å. All the TS's were confirmed by frequency analysis. ZPE was not considered in the present work since the vibrational analysis is not conducted for the IS due to its expensive computational requirements. Nonetheless, there is only one vibrational mode experienced a fundamental change between the IS and TS, and thus most vibrational energies between the IS and TS are offset (i.e., the reaction barrier of each elementary reaction will be only slightly affected with the consideration of the ZPE)<sup>8</sup>.

1. Kresse, G.; Hafner, J., *Phys. Rev. B* **1993**, 47 (1), 558-561; Kresse, G.; Hafner, J., *Phys. Rev. B* **1993**, 48 (17), 13115-13118; Kresse, G.; Furthmüller, J., *Computational Materials Science* **1996**, 6 (1), 15-50; Kresse, G.; Furthmüller, J., *Phys. Rev. B* **1996**, 54 (16), 11169-11186.
2. Blöchl, P. E., *Phys. Rev. B* **1994**, 50 (24), 17953-17979 ; Kresse, G.; Joubert, D., *Phys. Rev. B* **1999**, 59 (3), 1758-1775.
3. Perdew, J. P.; Yue, W., *Phys. Rev. B* **1986**, 33 (12), 8800-8802; Perdew, J. P.; Chevary, J. A.; Vosko, S. H.; Jackson, K. A.; Pederson, M. R.; Singh, D. J.; Fiolhais, C., *Phys. Rev. B* **1992**, 46 (11), 6671-6687.
4. Convergence test has been carried out with regard to the K-point sampling, energy cutoff and vacuum thickness till the difference of CO adsorption energies on each surface was less than 10 meV.
5. Gan, L.-Y.; Tian, R.-Y.; Yang, X.-B.; Lu, H.-D.; Zhao, Y.-J., *J. Phys. Chem. C* **2012**, 116 (1), 745-752.
6. Liu, P., *J. Chem. Phys.* **2010**, 133 (20), 204705.
7. Henkelman, G.; Uberuaga, B. P.; Jonsson, H., *J. Chem. Phys.* **2000**, 113 (22), 9901.
8. Fajin, J. L. C.; Cordeiro, M. N. D. S.; Illas, F.; Gomes, J. R. B., *J. Catal.* **2009**, 268 (1), 131-141.

Table S1. Lengths of the bond ( $d$ , Å) breaking/forming for TS, and imaginary frequencies ( $f$ ,  $\text{cm}^{-1}$ ) for the elementary steps of the WGS process on Cu(111), CuNi (111), and the inverse  $\text{NiO}_{1-x}/\text{CuNi}(111)$ .

	Cu(111)		CuNi (111)		$\text{NiO}_{1-x}/\text{CuNi}(111)$	
	$d$	$f$	$d$	$f$	$d$	$f$
$\text{H}_2\text{O}^* + ^* \rightarrow \text{H}^* + \text{OH}^*$	1.61	820	1.56	868	1.55	150
$\text{CO}^* + \text{OH}^* \rightarrow \text{cis-COOH}^* + ^*$	1.69	285	1.68	268	1.96	213
$\text{cis-COOH}^* \rightarrow \text{COOH}^*$	--	481	--	518	--	--
$\text{COOH}^* + ^* \rightarrow \text{CO}_2^* + \text{H}^*$	1.42	1398	1.48	1174	0.98	507

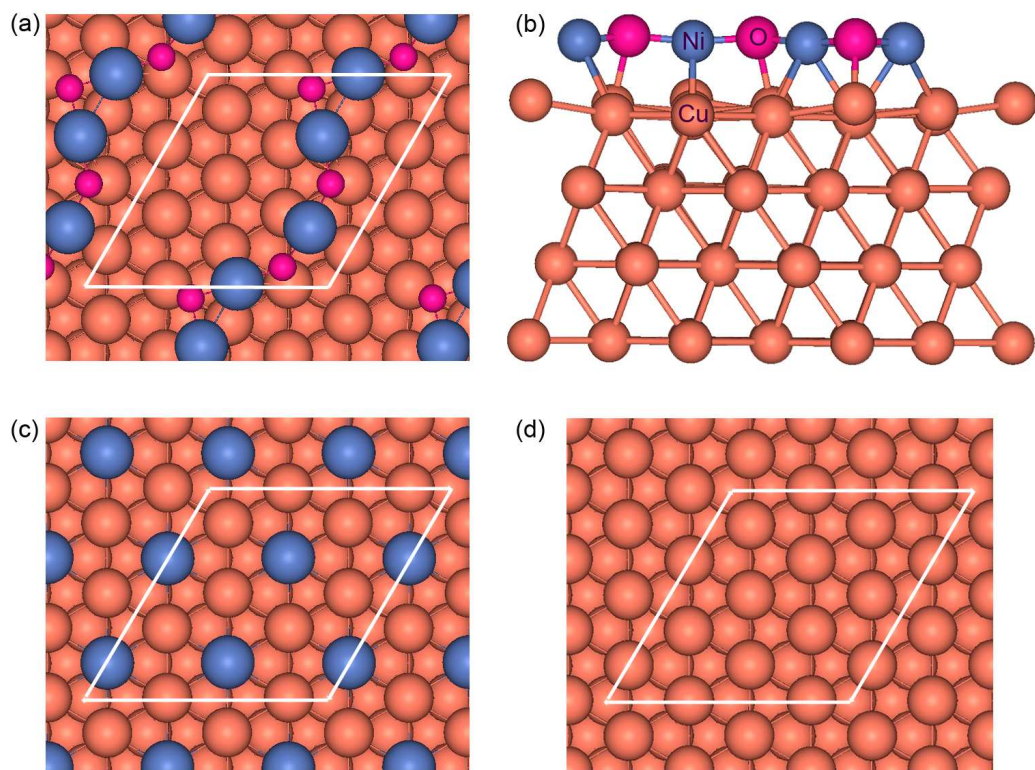


Fig. S1. (Color online) Top view (a) and side view (b) of fully optimized  $\text{NiO}_{1-x}/\text{Cu}(111)$  surfaces. Top view of  $\text{CuNi}(111)$  (c) and  $\text{Cu}(111)$  (d) surfaces. The  $(2\sqrt{3} \times 2\sqrt{3})R30^\circ$  unit cell is indicated by a white rhombus.

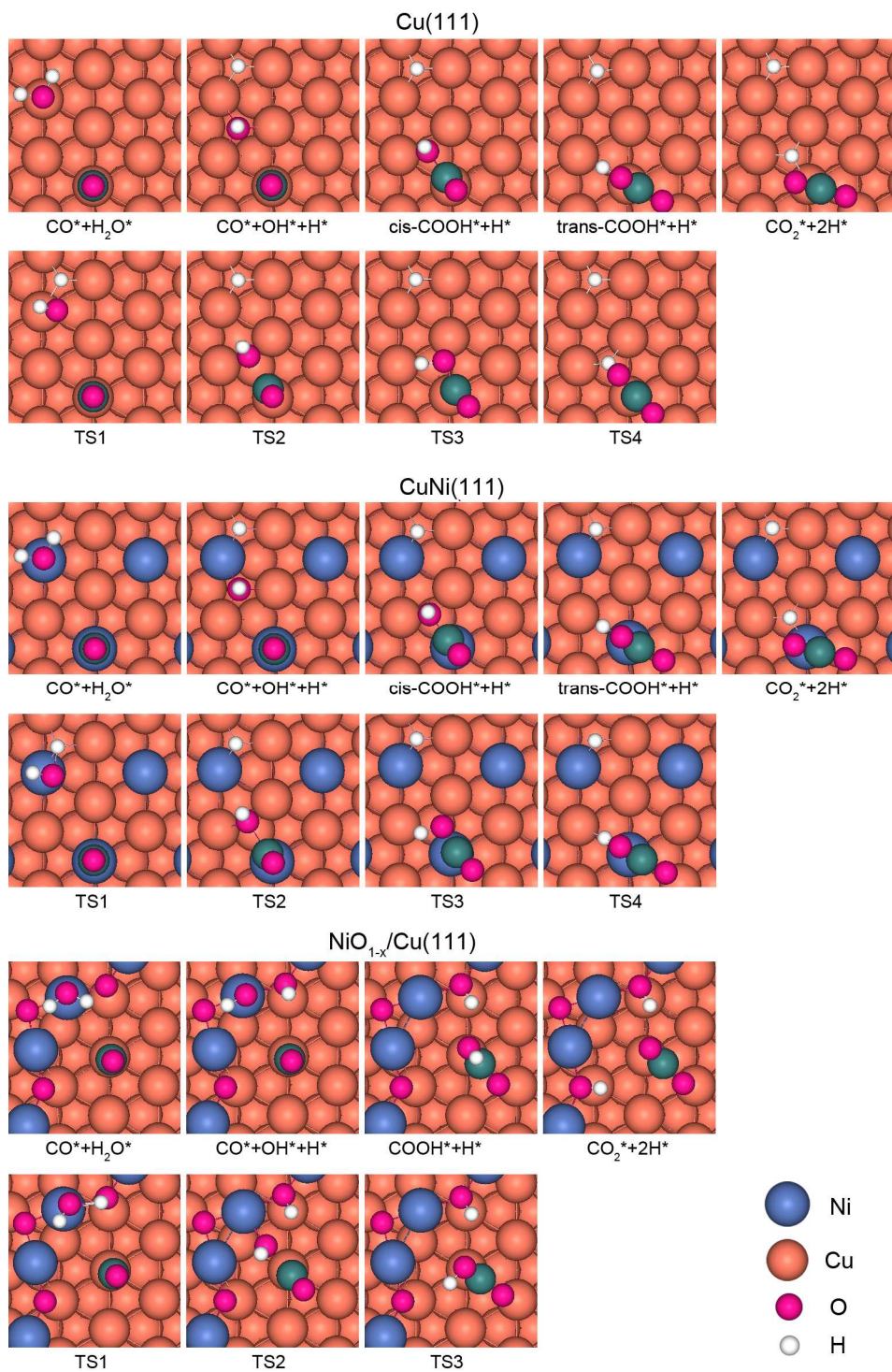


Fig. S2. (Color online) Optimized structures of local minima and corresponding transition states of the WGS process in Fig. 1 on Cu(111) (top panel), CuNi(111) (middle panel) and the inverse NiO<sub>1-x</sub>/Cu(111) (bottom panel).

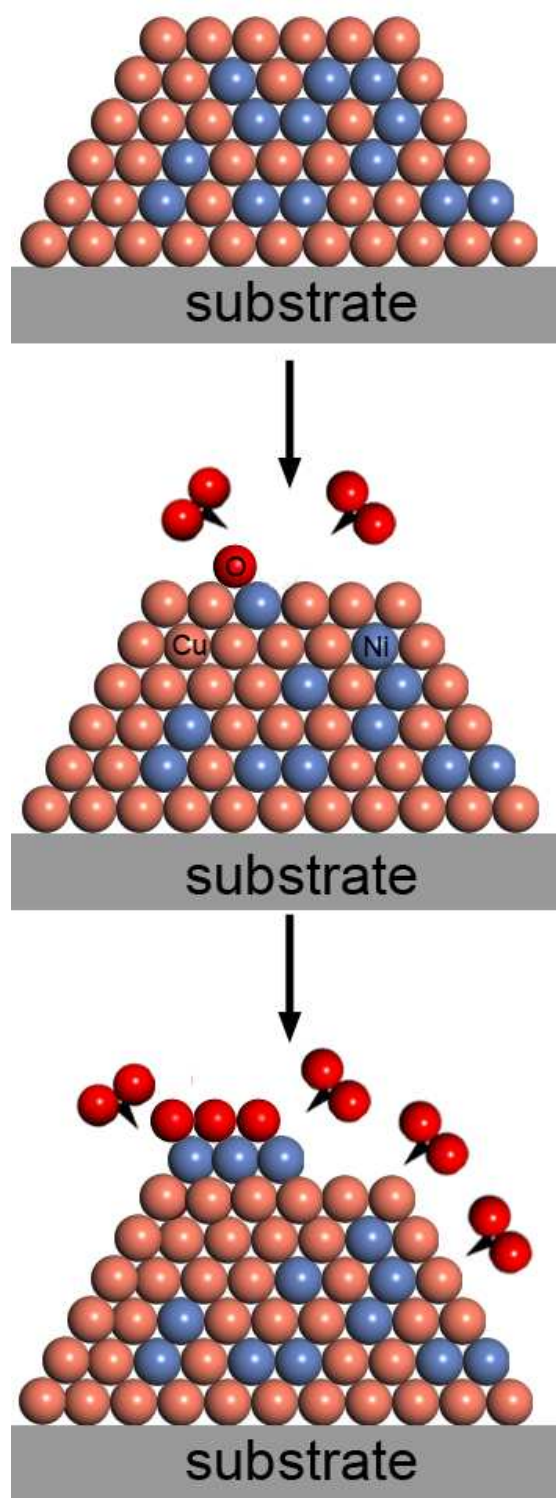


Fig. S3. (Color online) Possible process of synthesizing  $\text{NiO}_{1-x}/\text{Cu}(111)$  catalyst on a substrate.